AN ABSTRACT OF THE THESIS OF

Kenneth L. VandenBerghe for the degree of Master of Science in Chemistry on September 23, 1996.

Title: Solid State Luminescent Materials: New and Improved.

Redacted for Privacy

Abstract approved: _____

Douglas A. Keszler

The general emphasis of this work, has been synthesis, characterization, and optimization of solid-state luminescent materials. In particular, a study of $(Y,La)BO_3$ for use as a plasma display panel (PDP) phosphor, and the discovery and characterization of materials with the formula $M_4M'_2O_7F_2$ (M = Ca, Sr; M' = Si, Ge) have been undertaken.

The study of $(La,Y)BO_3$ focuses on the need for more efficient luminescent materials with better chromaticity (color) for PDPs. Phase equilibria in the system $LaBO_3$ - YBO_3 were examined at 1373, 1573, and 1773 K. On the basis of the results, compositions were selected for doping studies with the luminescent Eu^{+3} ion. Chromaticity values, excitation, and emission spectra were measured.

Synthesis and unit-cell parameters for new compounds with the formula $M_4M'_2O_7F_2$ are described. The structure is noted to contain oxygen atom that are bonded to three M atoms, which has been shown to produce unusual Eu^{+2} luminescence in borate compounds. The structure as well as Eu^{+3} and Eu^{+2} spectra are described.

Solid State Luminescent Materials: New and Improved

by

Kenneth L. VandenBerghe

A Thesis

submitted to

Oregon State University

in partial fulfillment of
the requirements for the
degree of

Master of Science

Presented September 23, 1996
Commencement June 1997

Master of Science thesis of Kenneth L. VandenBerghe presented on September 23, 1996

Approved:

Redacted for Privacy

Major Professor, representing Chemistry

Redacted for Privacy

Chair of Department of Chemistry

Redacted for Privacy

Dean of Graduate School

I understand that my thesis will become part of the permanent collection of Oregon State University libraries. My signature below authorizes release of my thesis to any reader upon request.

Redacted for Privacy

Kenneth L. VandenBerghe, Author

Acknowledgments

There are so many people to thank who have been instrumental in guiding me to this point. First, I would like to thank my parents, Lawrence and Louise, for all they have done. Who I am today, has been most influenced by their encouragement and support (both emotional and financial).

My role models growing up were my four brothers. Duane, Dan, and Keith have been fine examples to follow, and Brian has shown me what could be done with a little extra effort.

Since I have been in school for 21 years straight, a few teachers stand out in my memory as giving that extra effort, or showing me the light. Nelly Wegscheid and Dick Carmen are two of the nicest people I have ever met. Coaches Bob Bangston and Whitey Aus gave 110%, and encouraged me to, also. Lowell Roisum never stops surprising me (teacher, coach, principal, friend . . . maybe he should have run for president). My interest in science and chemistry started with 'Crazy' Craig Klawitter, and 'Big' Jim Sundstrom. I looked forward to Junior High Science, and excelled at Senior High Chemistry.

My time with the Bemidji Beavers was filled with fun and knowledge, mostly because of the excellent chemistry professors, Dr. Ken Lundberg and Dr. Gerald Morine. Dr. Kirt Dreyer, who has the worst fake German accent, gets a special thanks for being a good advisor, role model, and friend.

Dr. Matt Mattson and the gang from Notre Dame get a special thanks for kindness and patience shown to the summer help.

Dr. Michael Lerner made transition to graduate school painless, and started me on the road to research.

Dr. Doug Keszler, has been a great advisor; his enthusiasm, hard work, and never ending supply of ideas has made this thesis possible.

My fellow Keszler groupies; Dr. Annapoorna Akella, Dr. Junming Tu, and Dr. Jim Cox got me started and showed me the ropes. Jim tried to teach me to fish, and I tried to teach him to play basketball, neither of us were very successful. Anthony Diaz, Steve Crossno, Dong Li, Ki-Seog Chang, Kim Hockaday, and Greg Peterson are responsible for many insightful discussions on the how and why of chemistry, the state of the world, and last week's basketball game.

The friendship, encouragement, and humor provided by Dr. Rick Nafshun made it possible to get through grad school without going insane.

Special thanks to Emily, Lura, and Alexandra for putting up with a sometimes grumpy, lazy, messy, cranky, me.

Finally, thanks to Natalie for being there for me during the good and the bad times. Her level of attention to details, knowledge, and self sacrifice are goals I wish to achieve.

CONTRIBUTION OF AUTHORS

The vacuum ultraviolet (VUV) spectra in Chapter 2 were obtained in the lab of Dr. Richard Meltzer at the University of Georgia.

The work on the synthesis, data, and structure solution of $Sr_4Ge_2O_7F_2$, in chapter 3, was preformed by Annopoorna Akella, as was Figure 3.2, polyhedra of the Ge_2O_7 groups. I performed the synthesis, structure determinations, and luminescence measurements of the rest of the materials.

TABLE OF CONTENTS

LIST OF FIGURES

LIST OF FIGURES (Continued)

LIST OF TABLES

Solid State Luminescent Materials: New and Improved

Chapter 1
Introduction

Luminescent materials have widespread use in today's modern world, including television, computer monitors, oscilloscopes, fluorescent lights, photocopy machines, suntan lamps, X-ray and γ-ray detectors (1), and bug zappers. Wonder how a laundry detergent can get your clothes 'whiter than white'? Include a white luminescent material with the detergent, and when you look at your 'clean' clothes they not only look white, they emit white light. I watched a sanitation worker pour a red luminescent material down a home owners drain, and then go sit in the dark sewer looking for the red luminescence, to determine if the drain was connected to the sewer. The *Indiglo®* watch uses a luminescent screen behind its face, instead of a light bulb, for illumination in the dark. Flat panel television is nearing commercialization, thinner and lighter than present televisions, with the ability to hang on the wall. These new televisions will have the advantage of wider, brighter screens (2). Once the flat panel television is developed, imagine the other possibilities, every gauge in your car will be on one display, good quality virtual reality headsets, signs that are changeable displays. Why use fluorescent lights? Imagine a light-weight emissive panel that covers the entire ceiling.

As you can see, there are plenty of reasons for developing newer, better luminescent materials for today's and tomorrow's needs. The emphasis of my work has been the improvement of a currently used material, and the development of a new one.

$(Y,Gd)BO_3$ doped with Eu^{+3} is currently being used as the red component of plasma display televisions. By introducing La into the material we hope to improve its excitation and emission properties. New materials with the formula $M_4M'_2O_7F_2$ (M = Sr, Ca; M' = Si, Ge) were discovered, the crystal structure solved, and luminescent properties examined.

Solid Solutions

"Often certain properties of materials... are modified by changing the composition in such a way that a solid solution forms and great use may be made of this in designing new materials that have specific properties (3)." A solid solution is just what the name implies, a solution of materials that happens to be a solid. Just like with liquid solutions, it is a homogeneous phase that has a variable composition. Many alloys are really a solid solution, for example brass is a mix of copper and zinc.

There are two types of solid solutions, substitutional and interstitial. Interstitial solid solutions are formed by placing atoms between those that are already present. As long as the inserted atoms are small enough to fit in existing holes, large amounts may be inserted with minimum change to the original structure. Substitutional solid solutions are formed by substituting one type of atom for another. If the atoms are similar in size and charge, then the structure will remain the same; however, if the atoms are too different, and enough of them are substituted, the structure is forced to change. This is the type of solution we expect, by substituting La for Y in YBO_3, because of the large size difference. Ideally, if the structures are the same for the two end compounds, a linear change in the

size of the unit-cell (and the properties) is seen by changing the composition. If the two end structures are different, then at some point the solubility limit will be reached, and at this point both structures form. See figure 1.1. The real world is seldom ideal, and the behavior of solid solution is no exception. Deviations from linearity, gradual changes at the solubility limit, multiple phases or structures, interstitial and substitution, vacancies, and heterogenous mixtures can all make interpretation of data complex.

My interest in solid solutions focuses on $(Y,Gd)BO_3:Eu^{+3}$, which has good luminescent properties, that can be modified by substitution of La.

Eu^{+3}

The red luminescence of Eu^{+3} has been well characterized in the literature (4, 5, 6). Shifts in the position of the luminescent peaks, from sample to sample, is always minimal, because of the electron configuration. Since the configuration of Eu^{+3} is $4f^6$ the HOMO to LUMO transition is f to f. These orbital are protected from the surroundings by filled 5p and 5s orbitals, and as a consequence do not see much crystal field splitting. Since there is little crystal field splitting, the excited state and ground state are very similar, and emission is a narrow band. See figure 1.2. Changes in the spectrum of Eu^{+3} perhaps have more to do with the symmetry of the Eu site. Sites with inversion symmetry, only allow magnetic-dipole transitions ($\Delta J = \pm 1$), which is the $^5D_0$ - $^7F_1$ transition ($\approx$5900Å), usually too orange for most applications. However if the site symmetry is noncentrosymmetric, the electric-dipole transition is allowed ($\Delta J = \pm 2$), which is the $^5D_0$ - $^7F_2$ transition

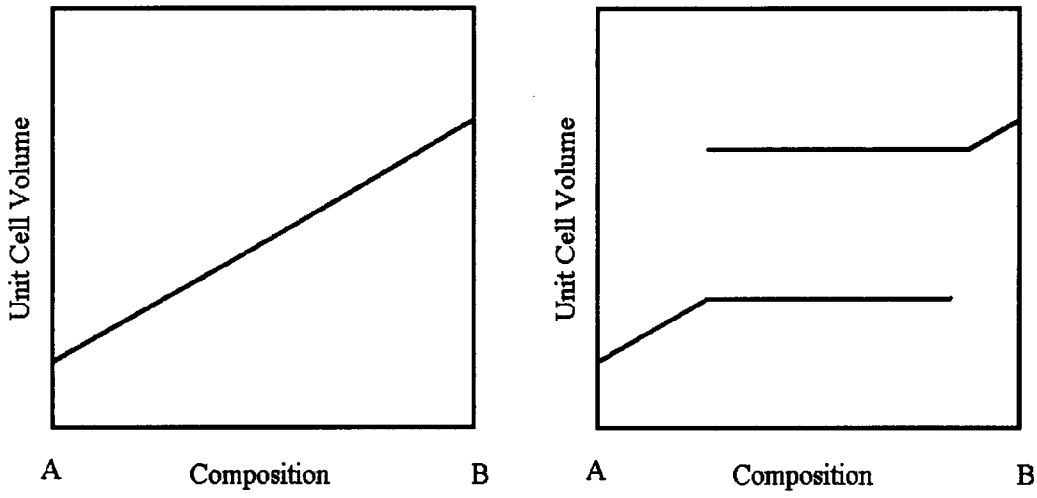

Figure 1.1 If compound A and B are the same structure, and similar in size, a continuous solid solution can be formed. If the compounds are unique enough, only limited solubilities can be reached, at which point both compounds will exist.

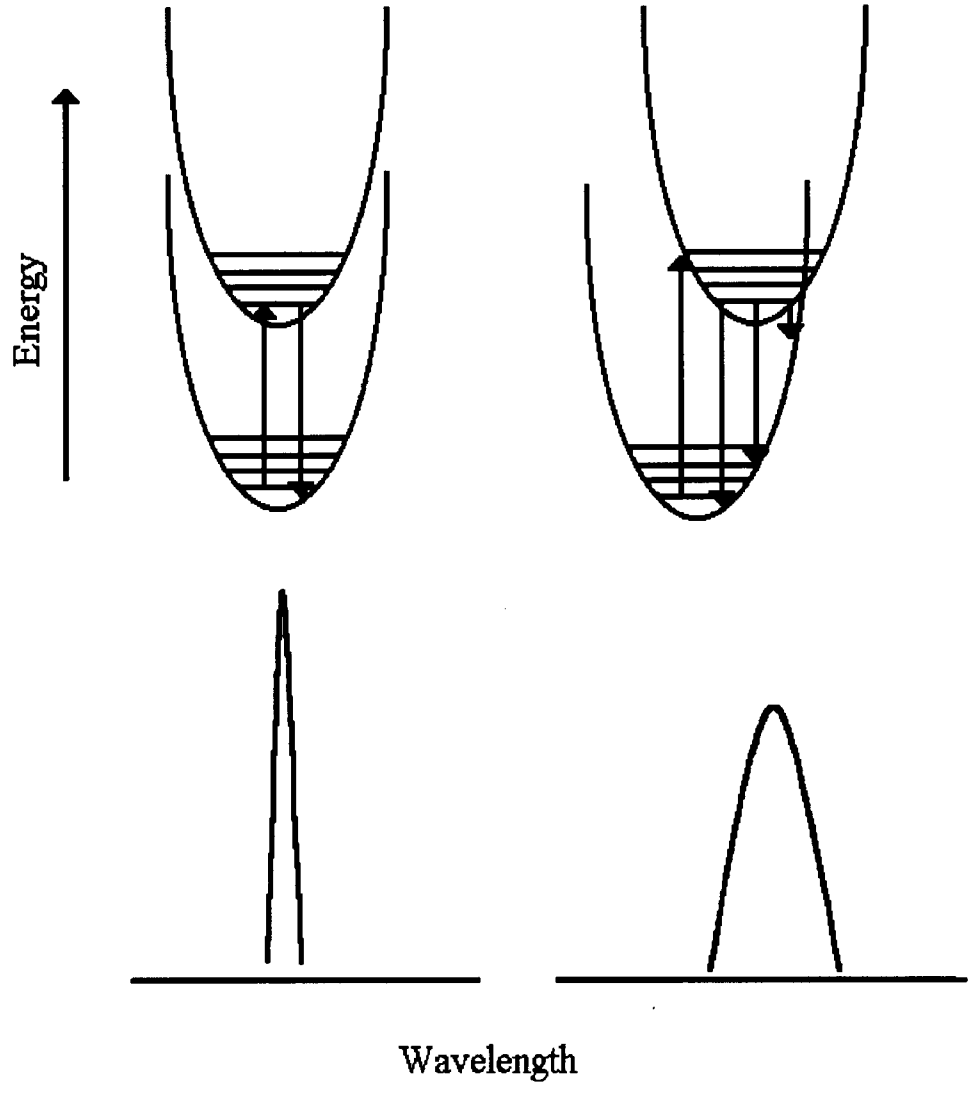

Figure 1.2 Configurational coordinate diagram for Eu^{+3} and Eu^{+2}. Since Eu^{+3} has a small Stokes shift, the transition from the excited state to the ground state occurs at approximately a single energy, producing a sharp peak. The Eu^{+2} transition has a wide range of energy values because of the strong vibronic coupling, producing a broad peak.

(≈6200Å), the perfect red. As the symmetry around the Eu site changes so do the intensities of all the transitions.

My interest in Eu^{+3} comes from the fact that many commercial red phosphors use Eu^{+3}. It can be very bright and efficient, and has the desired emission wavelength. It also has unique properties based on the environment around it, which can lead to structural information.

Eu^{+2}

Luminescence from Eu^{+2} can be more unpredictable than Eu^{+3}, but not any less investigated or important (7, 8, 9). The electron configuration is $4f^7$ and typically shows a $5d^14f^6 \rightarrow 4f$ transition emission, that can vary from ultraviolet to red. Since the 5d levels are not shielded like the 4f levels, the surrounding environment plays a large part in determining the emission wavelength. The excited state is now going to be different from the ground state, and a broad band that can be Stokes shifted a little or a lot, is seen as emission. See figure 1.2.

The variability in the emission wavelength of the Eu^{+2} makes it an interesting dopant. If control of the wavelength can be achieved, while retaining high brightness, many commercial phosphors could be replaced.

Spectra and Spectrometer

Luminescence spectra were obtained from the spectrometer depicted in figure 1.3. Excitation radiation was supplied by a 400 watt Xe lamp, passed through a 50 centimeter

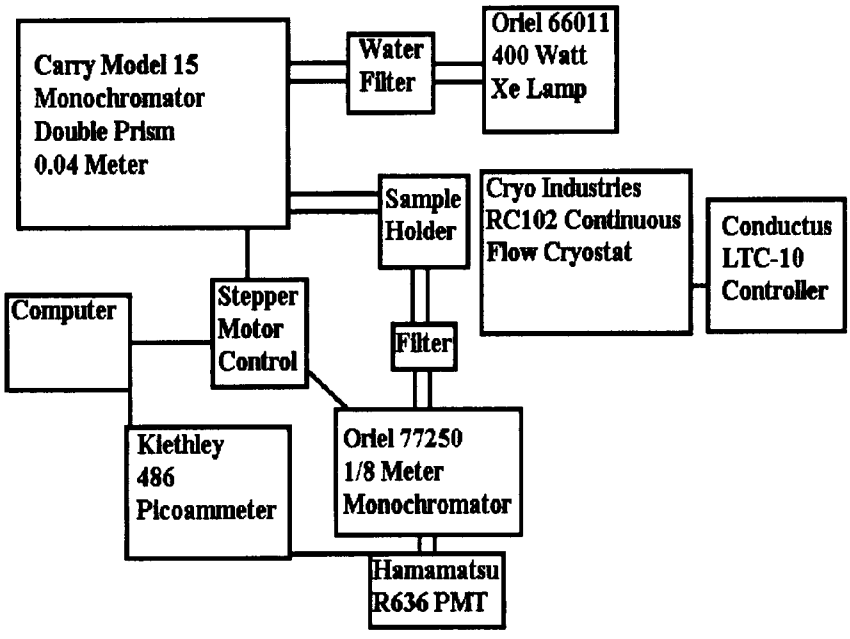

Figure 1.3 The spectrometer used in the Keszler lab.

water filter (to remove IR radiation), into a double beam 0.04 meter monochromator, and then to the sample. Emission was collected with a Hamatasu R636 Photomultiplier tube after radiation was passed through a filter (to remove excitation radiation), and a 1/8 meter grating monochromator. The signal was converted for computer acquisition with a picoammeter. Control of the monochromators and data collection were preformed with software written in this laboratory. Excitation spectra corrections were made by using rhodamine B (2300-3300Å) and sodium salicylate (3200-4000Å) as constant quantum counters. Emission spectra corrections were made with a calibrated tungsten lamp from Eppley Laboratories. Low-temperature spectra were obtained in the same manner, except the sample holder was replaced by a continuous flow cryostat sample cell. Sample were mounted in the cell, evacuated, and cooled to temperature.

Chapter 2
$Y_{1-x}La_xBO_3$

Abstract

Phase equilibria in the system $LaBO_3$-YBO_3 has been studied by using standard solid-state preparative methods and X-ray diffraction techniques; solid solubilities were examined for samples synthesized at 1373, 1573, and 1773 K. Unit-cell volumes were determined for each temperature, and an approximate phase diagram was constructed. Chromaticity values and excitation and emission spectra of the Eu^{+3}-doped solid samples were obtained for comparison to a commercially available phosphor.

Introduction

With the arrival of Plasma Display Panels (PDP) comes the need for new phosphors with properties that match the needs of this new industry. Most phosphors used for television, fluorescent lamps, and scintillators do not have the desired characteristics needed for a good PDP phosphor (9,10). Commercial PDP phosphors will have high absorbance of 1470Å excitation radiation (the emission of the xenon plasma), efficient transfer of the energy absorbed to the sensitizer ion, high quantum efficiency of the sensitizer at the desired emission wavelength, inexpensive starting materials, and low cost/ ease of production. This study concentrates on improving the existing phosphor $(Gd,Y)BO_3$:Eu^{+3}, (which is centered at 1650Å, and only 85% of the maximum height at

1470Å). See figure 2.1. To achieve optimum overlap of the Xe emission, the absorption peak needs to be centered at 1470Å . This peak is thought to be absorption of energy by the borate group. La has been partially substituted for Y, since La is more electropositive, the La-O bond distance is longer then the Y-O distance. The connected O should then have more electrons to share with the B atom, and the B-O bond should be shorter, therefore higher energy absorbing. See figure 2.2. The chromaticity of the emission is not ideal for a good red color, being too orange for commercial use. Examining the $YBO_3:Eu^{+3}$ emission spectrum, the splitting of peaks is consistent with J level splitting of site symmetry approximating octahedral. See figure 2.3. By inserting x% La into the structure, the octahedral symmetry should be relaxed, changing the splitting of the emission peaks and the chromaticity. A solid solution of $LaBO_3$ and YBO_3 was prepared at varying compositions and temperatures. The solubilities, phase diagram, and the excitation and emission spectra, and the chromaticity values for Eu^{+3} doped samples are presented here.

Experimental

Powders of the solid solution were synthesized by using standard high-temperature solid-state methods. Stoichiometric quantities of Y_2O_3, La_2O_3, and B_2O_3 were mixed with a 5-wt% excess of B_2O_3 (compensation for water, boric acid contamination, and B_2O_3 evaporation), ground under hexane, and heated in a platinum crucible to 1073 K for 30 minutes. The samples were reground and heated for one hour at 1273 K, reground and heated to final temperature for 10 to 24 hours. Samples heated to 1773 K were covered

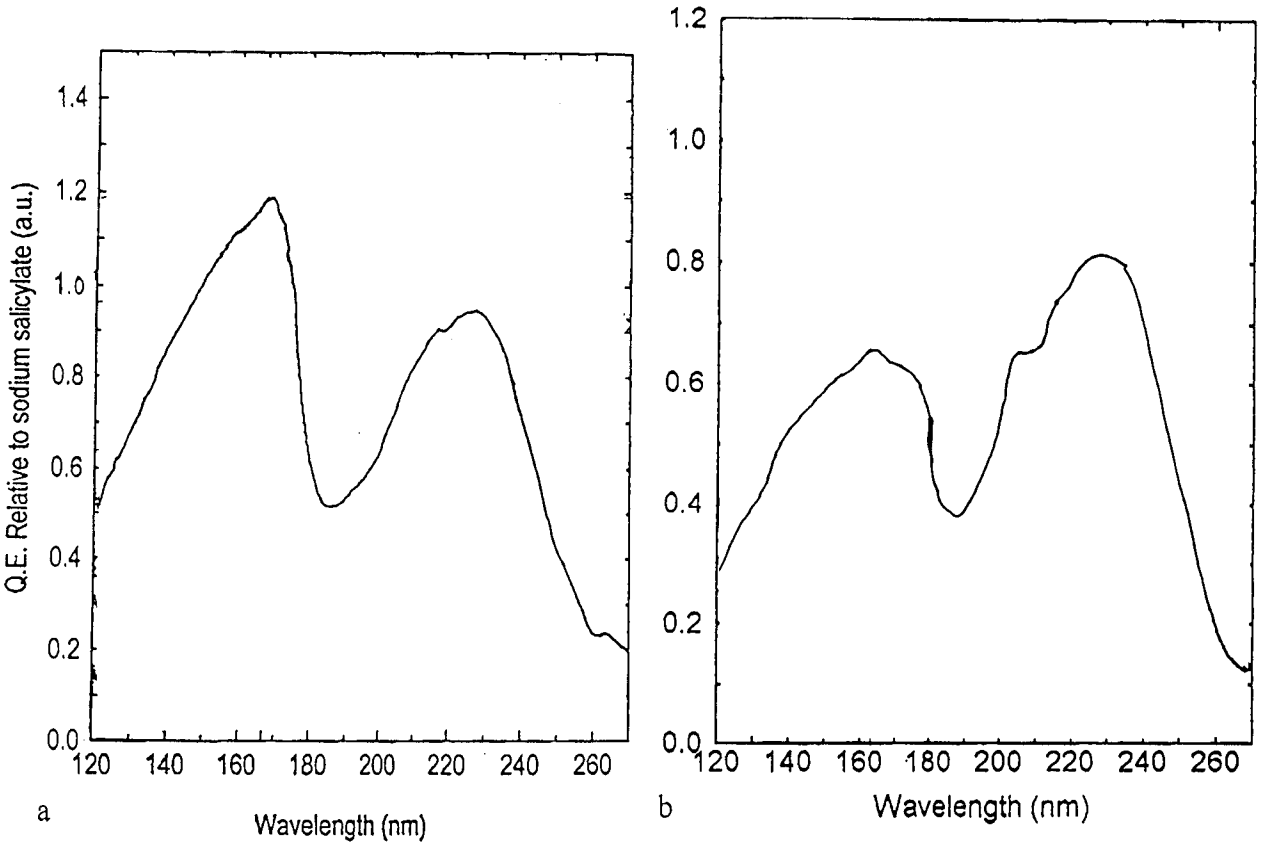

Figure 2.1 Vacuum ultra violet (VUV) excitation spectrum of a) $(Gd,Y)BO_3:Eu^{+3}$, and b) $Y_{0.75}La_{0.25}BO_3:Eu^{+3}$. Note the maximum peak height and the height at 147nm.

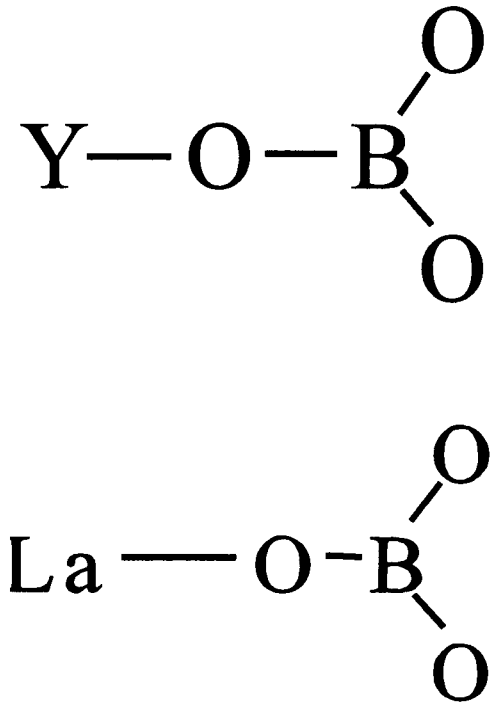

Figure 2.2 The longer La-O bond makes the adjoining B-O bond shorter and higher energy absorbing.

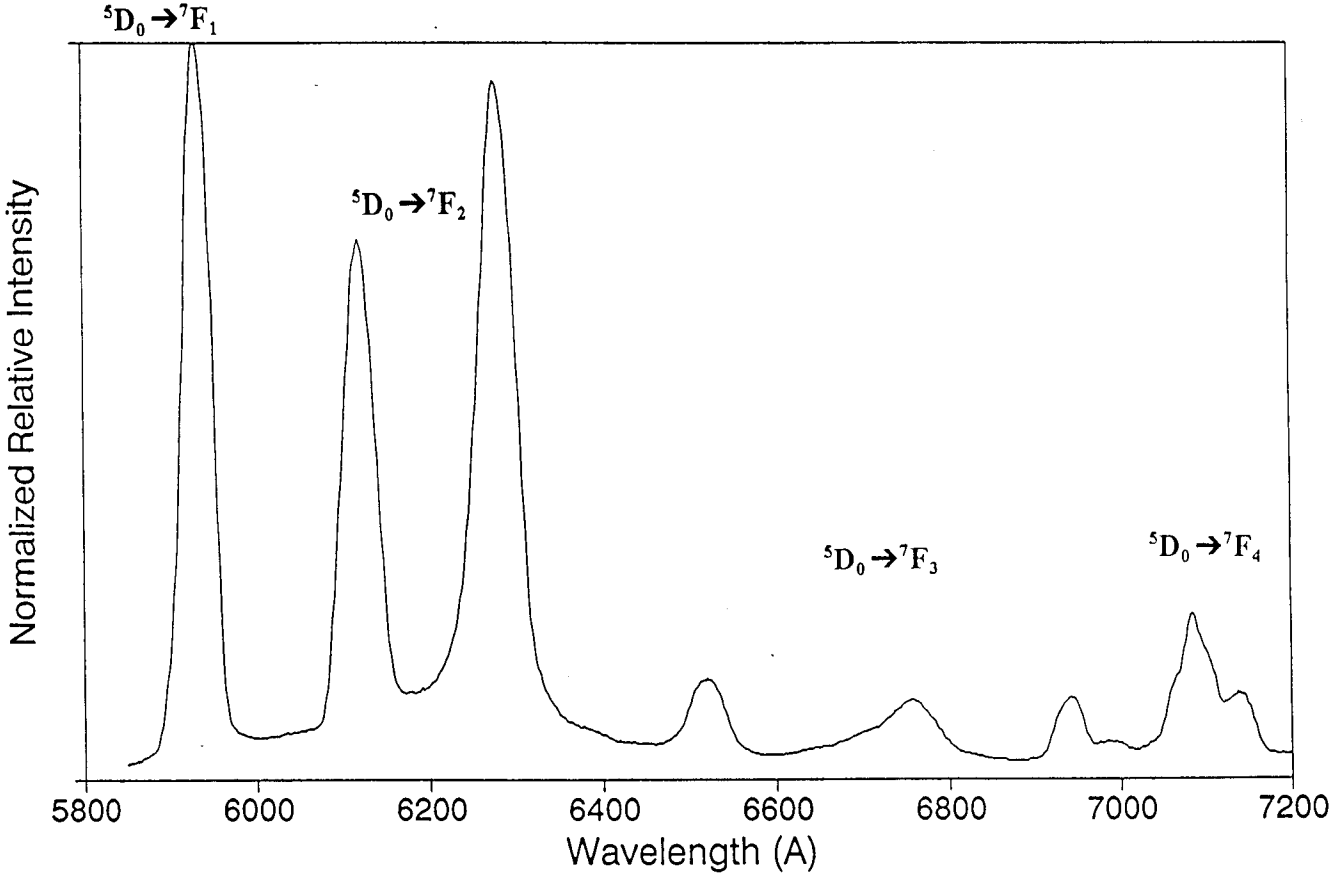

Figure 2.3 Transition of YBO_3 doped with 3% Eu^{+3}. Excitation at 3940Å.

with a platinum lid to reduce volatilization of B_2O_3 and prevent formation of M_3BO_6. Eu^{+3} samples were prepared with 1.5 mol% doping of Eu_2O_3.

Powder X-ray data were collected on an automated Philips diffractometer. Peak positions were corrected by using an internal silicon powder standard. Positioning of peaks and unit-cell parameters were refined with the least squares computer program *POLSQ* (11). Emission spectra were collected on the system described in chapter one. Vacuum ultraviolet (VUV) excitation spectra were collected at the University of Georgia by members of Dr. Richard Meltzer's research group. Chromaticity values were calculated by using a computer program designed in-house, modeled from a standard chromaticity table (12).

Results and Discussion

At 1373 K, the maximum solubility of La in the YBO_3 structure is approximately 10 mol% (cf. figure 2.4). The solubility of Y in $LaBO_3$ is also approximately 10 mol%, and at concentrations between these values both the YBO_3 and $LaBO_3$ phases are seen by powder X-ray diffraction. Samples prepared at 1373 K are not well crystallized, and the diffraction peaks are not sharp or well defined; consequently, the calculated unit-cell volumes from sample to sample are not consistent and have large standard deviations.

At 1573K, the maximum solubility of La in YBO_3 is between 20 mol% and 30 mol%; at concentrations higher then 30% new phases appear. Both the high temperature (HT) $NdBO_3$ and HT $LaBO_3$ phases coexist up to 80 mol% La. The low temperature (LT)

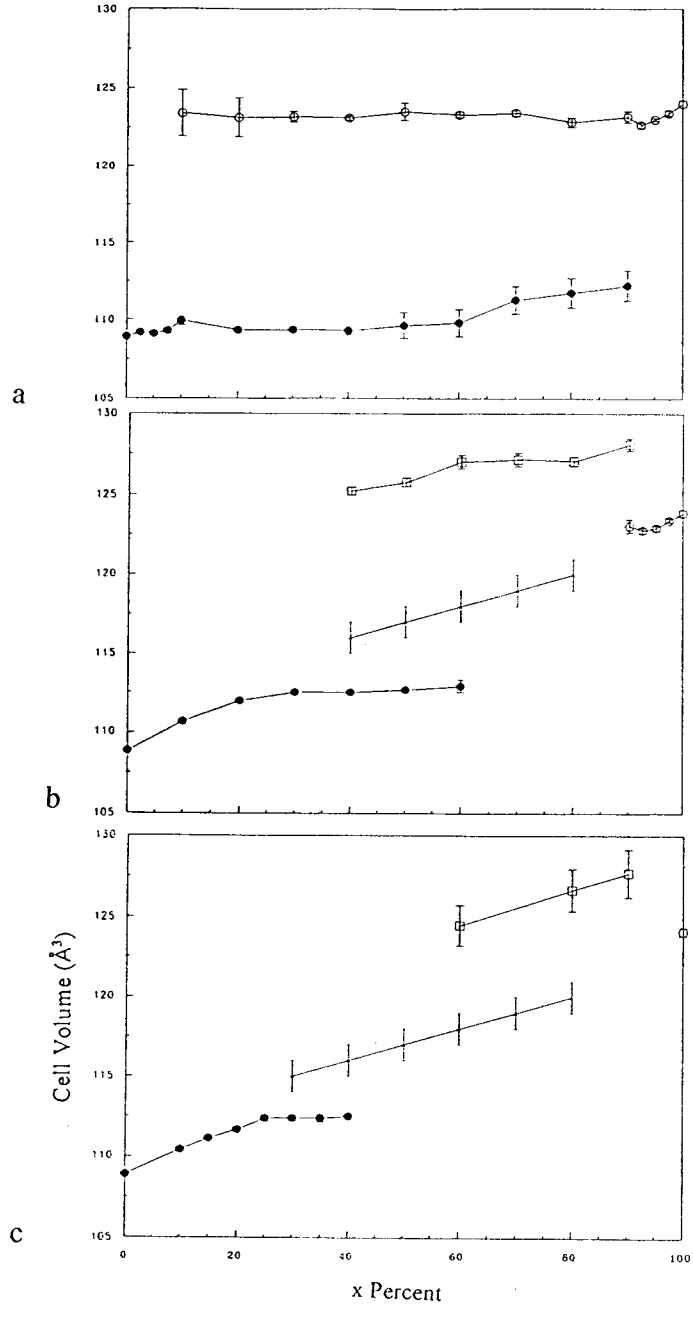

Figure 2.4 $Y_{1-x}La_xBO_3$ solid solution data at a) 1373 K b) 1573 K c) 1773 K. The solid circles are YBO_3 phase, open circles are LT $LaBO_3$ phase, squares are Ht $LaBO_3$ phase, and small dots are HT $NdBO_3$. The Lt $LaBO_3$ cell volumes have been divided in half for display purposes (Z = 4, but for all others Z = 2). Since the structure is not known for HT $NdBO_3$, data are displayed only to show the approximate relation between the increase in La concentration and increase in cell volume.

$LaBO_3$ phase exists from 80 mol% through 100 mol% La. Between 20 mol% and 7.5 mol% Y both the HT and LT forms of $LaBO_3$ are present (cf. 2.4 and 2.5).

At 1773 K, La solubility in YBO_3 reaches a maximum at approximately 25 mol%. From 25 mol% to 80 mol% La substitution the HT $NdBO_3$ phase is present, the low end of this range also shows the YBO_3 phase. At 50 mol% La addition only the $NbBO_3$ phase is present. Sixty percent La substitution shows the HT $LaBO_3$ phase and is present until greater than 90 mol%. The transition from LT to HT $LaBO_3$ occurs between 0 mol% and 10 mol% Y substitution, and in pure $LaBO_3$ at temperatures between 1773 and 1823 K (cf. 2.4 and 2.5).

YBO_3 structure has not been solved by single crystal methods; however, many structures have been proposed (pseudo wollastonite, vaterite, pseudo vaterite . . .) (13, 14, 15). Attempts are currently being made, by our group, to grow single crystals for structure solution. The structure assumed here is vaterite, a hexagonal unit-cell with parameters of a = 3.77, c = 8.81, volume = 108.9, and Z = 2 (all values are in Å or $Å^3$). There are assumed two Y sites one with octahedral symmetry, and one with 6 + 6 coordination. The latter is a six coordinate site with six additional weaker bonds at longer distances (16). The number of peaks from the Eu^{+3} spectra is consistent with the J level splitting predicted from approximate octahedral symmetry (O_h) of the Y site. The $^5D_0$ - $^7F_1$ transition shows only one peak, the $5D_0$ - $^7F_2$ is a doublet of peaks, the $^5D_0$ - $^7F_3$ shows three peaks and the $^5D_0$ - $^7F_4$ yields four peaks. The $^5D_0$ - $^7F_0$ is too weak to be observed. See figure 2.3.

The LT and HT $LaBO_3$ phases differ only slightly in structure as seen in figure 2.6. Both have single nine coordinate La sites; However, the LT cell has higher symmetry being orthorhombic with parameters of a = 5.15, b = 8.30, c = 5.88, volume = 250.4, Z

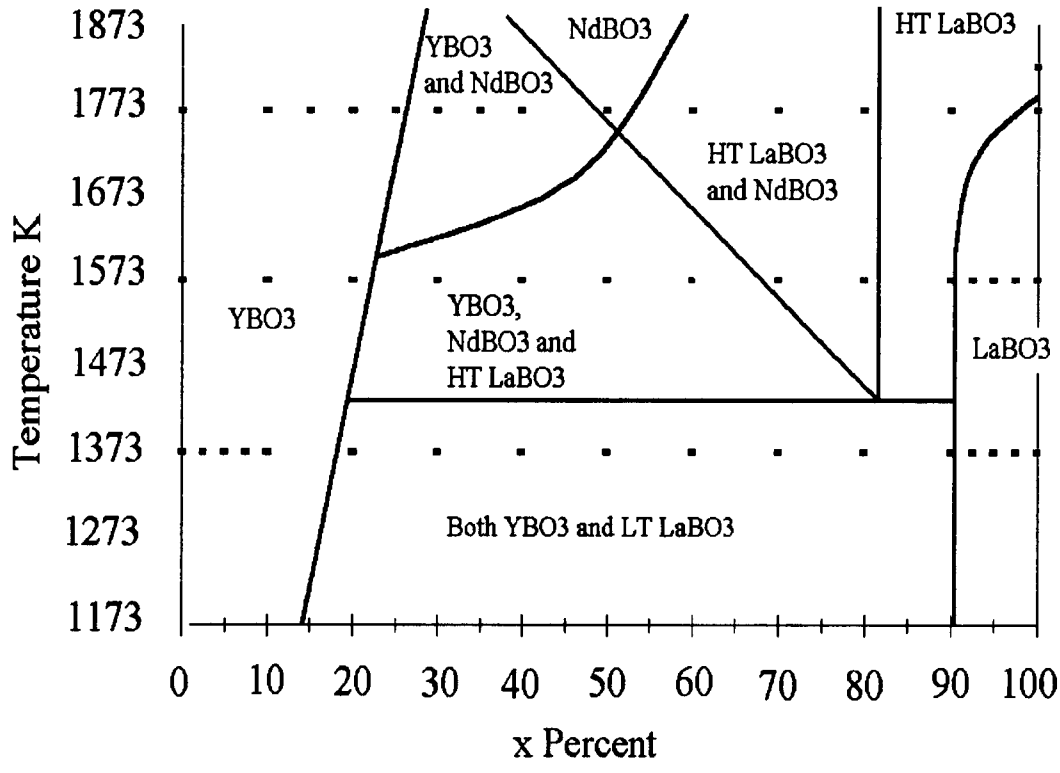

Figure 2.5 Phase diagram for the $Y_{1-x}La_xBO_3$ solid solution. All data points are taken from analysis of X-ray powder diffraction data.

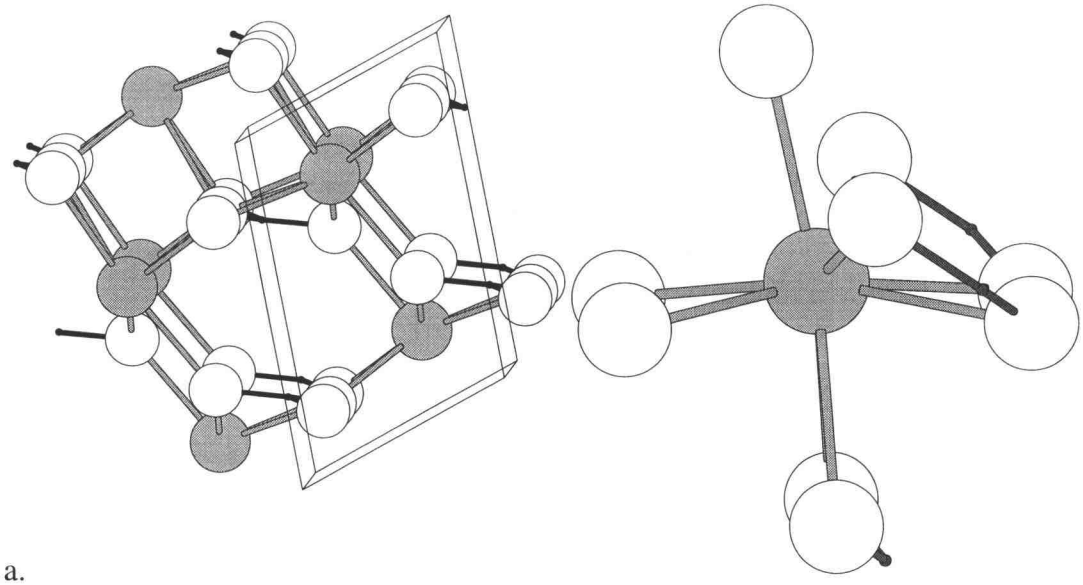

a.

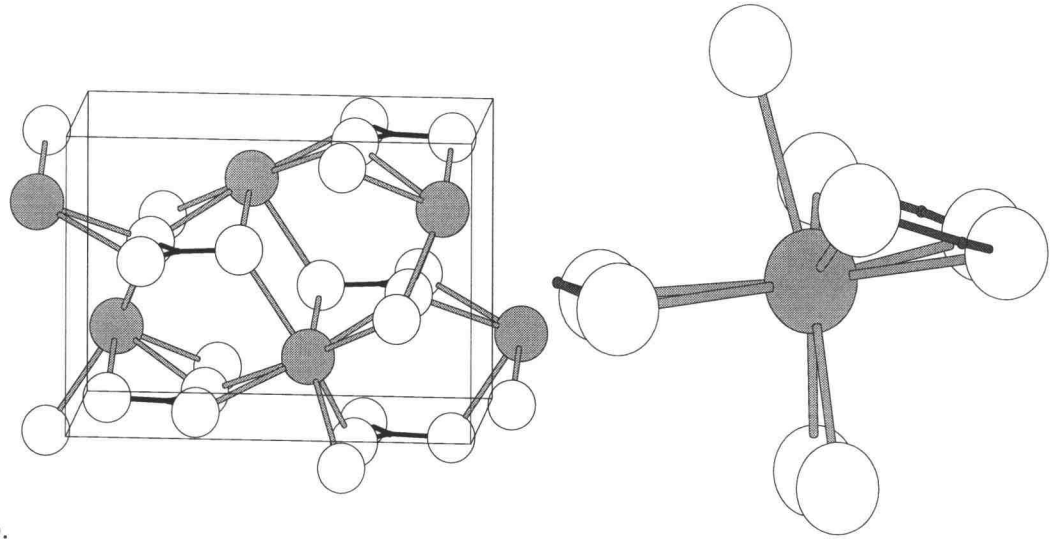

b.

Figure 2.6. a). HT $LaBO_3$ b). LT $LaBO_3$ Large shaded circles represent La atoms, open circles represent O, and small black circles represent B atoms. Unit-cell with cyclic $(La\text{-}O\text{-}B\text{-}O)_2$ group and nine coordinate La site.

= 4 (17). The HT cell is monoclinic with a = 6.35, b = 5.08, c = 4.19, $\beta = 107.9^{O}$, Z = 2 (18). Eu^{+3} spectra are shown in figure 2.7.

From the Eu^{+3} emission spectrum the HT phase of $NdBO_3$ appears to be an intermediate of the YBO_3 and high temperature $LaBO_3$ (perhaps seven or eight coordinate?). See figure 2.7. No structural data are available in the literature, but by examining the unique HT $NdBO_3$ powder diffraction peaks, higher concentration of La shifts peaks to lower values of two theta. This is consistent with substitution of the larger La atom increasing the unit-cell.

Chromaticity values for several compounds are listed in table 2.1. The Y_2O_3:Eu^{+3} X and Y values are close to the ideal commercial red values. The solid solution chromaticity values are not ideal, but a change was seen by removing the octahedral symmetry of the Eu site in YBO_3, to distorted Eu site at the maximum La solubility of $Y_{0.75}La_{0.25}BO_3$.

As can been seen from figure 2.1, the excitation peak for $Y_{0.75}La_{0.25}BO_3$ is centered at 1620Å, and at 1470Å is 90% of the maximum intensity. This corresponds to a 5% increase, over the $(Gd,Y)BO_3$, in the peak width at 1470Å compared to the maximum peak height; however, overall there is about a 40% decrease in the peak height at 1470Å.

Acknowledgments

This work was supported by the Phosphor Technology Center of Excellence (PTCOE).

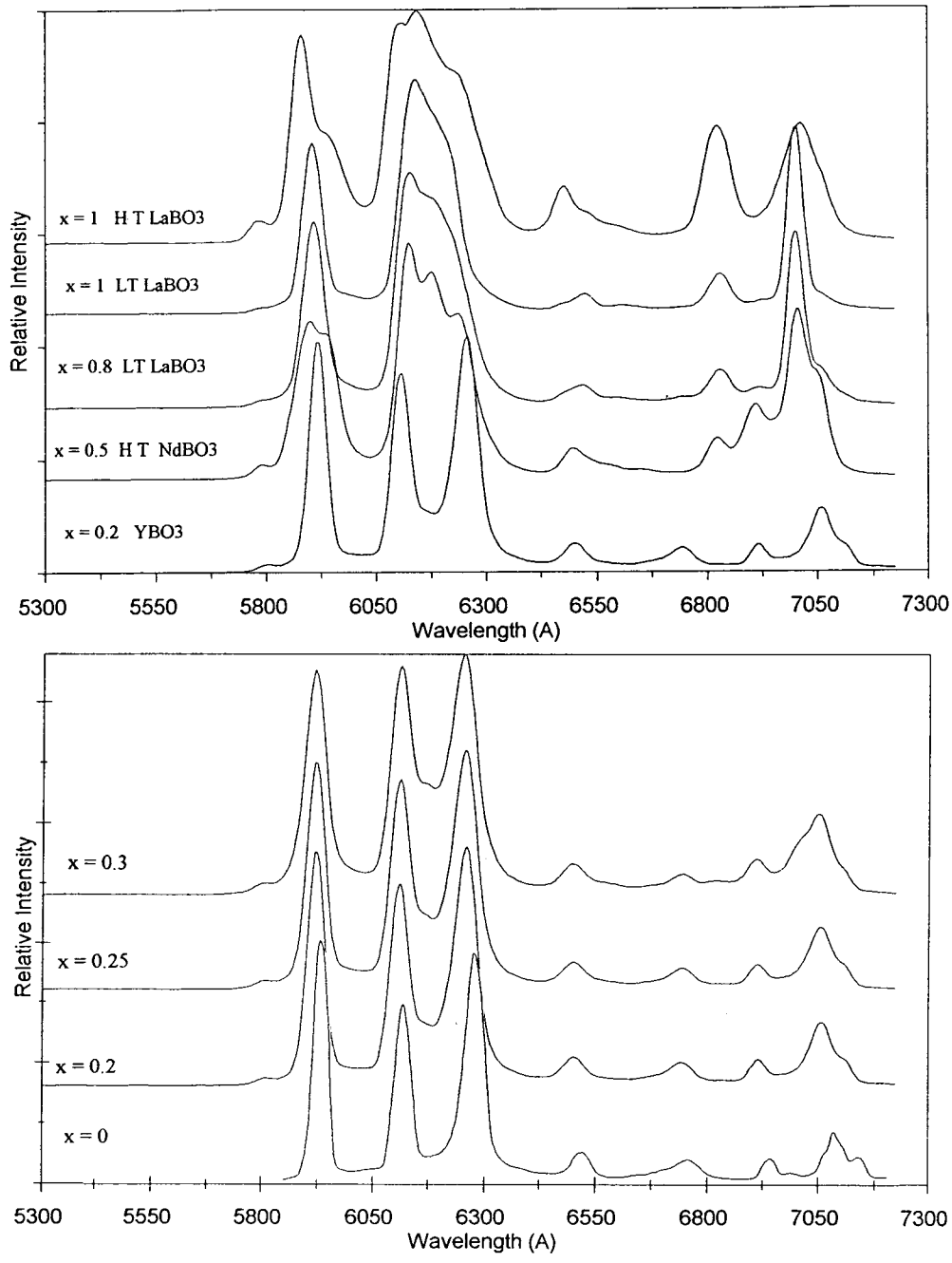

Figure 2.7 Emission spectra of $Y_{1-x}La_xBO3:Eu^{+3}$ samples, excitation at 3970Å.

Table 2.1 Chromaticity values calculated from Eu^{+3} emission data. Values similar to Y_2O_3:Eu^{+3} are acceptable for a commercial red.

Formula	Phase	X	Y
Y_2O_3	Y_2O_3	.654	.346
YBO_3	YBO_3	.637	.362
$Y_{0.8}La_{0.2}BO_3$	YBO_3	.648	.352
$Y_{0.75}La_{0.25}BO_3$	YBO_3	.648	.352
$Y_{0.7}La_{0.3}BO_3$	YBO_3	.647	.353
$Y_{0.5}La_{0.5}BO_3$	HT $NdBO_3$	.643	.357
$Y_{0.2}La_{0.8}BO_3$	LT $LaBO_3$	.648	.350
$LaBO_3$	LT $LaBO_3$	.649	.351
$LaBO_3$	HT $LaBO_3$	.650	.351

Chapter 3
Structure, Eu^{+2}, and Eu^{+3} Luminescence of $M_4M'_2O_7F_2$ (M=Sr,Ca; M'=Ge,Si)

Abstract

The new compound $Ca_4Si_2O_7F_2$ with unit-cell dimensions of a = 7.534(8), b = 10.535(1), c = 10.902(1)Å, β = 109.553(8)°, V = 815.6(2)Å^3, was determined by single crystal X-ray methods. The isostructural compound $Sr_4Ge_2O_7F_2$ whose unit-cell dimensions a = 8.024(1), b = 11.224(1), c = 11.547(2)Å, β = 109.79(1)°, V = 978.6(3)Å^3 was also determined by X-ray analysis. $Ca_4Ge_2O_7F_2$ was prepared, and has unit-cell parameters of a = 7.66, b = 10.72, c = 11.24Å, β = 109.8°, V = 868.4Å^3 calculated by powder X-ray methods. The structure, Eu^{+3}, and Eu^{+2} luminescence are described.

Introduction

Searching for $LiCa_2SiO_4F$, crystals of $Ca_4Si_2O_7F_2$ were grown, and the structure was determined by single crystal X-ray analysis. Crystals of $Sr_4Ge_2O_7F_2$ were found to be isostructural, also by single crystal X-ray analysis. Switching metal atoms, the combination $Ca_4Ge_2O_7F_2$ was also found to be isostructural, but the $Sr_4Si_2O_7F_2$ combination was found not to exist.

The relationship of oxygen bonded to 3 or more large heavy atoms (Sr or Ba) has been shown to produce an unusually large Stokes shifted emission in borate compounds when doped with Eu^{+2} (19). Six of the seven oxygen, in the structure studied here, are bonded to three M atoms and one M'. Fluoride atoms, which are similar to oxygen size

and electronegativity, also have four bonds to M atoms. Similar Stokes shift are observed, when doped with Eu^{+2} as with the borates.

The structure, Eu^{+2}, and Eu^{+3} spectra are shown here.

Experimental

A $Ca_4Si_2O_7F_2$ crystal was obtained by heating 2 molar equivalents $CaCO_3$ and 1 equivalent SiO_2 to 1073 K in a Pt crucible for 4 hours. The sample was reground and heated to 1373 K for 10 hours. One equivalent of LiF was added and the mixture was heated, under a N_2 atmosphere, to 1273 K for 8 hours. The melt was allowed to cool naturally by turning off the power to the furnace. A crystal of $Sr_4Ge_2O_7F_2$ was obtained by heating and slowly cooling stoichiometric quantities of $SrCO_3$, GeO_2, and SrF_2 in a platinum crucible under an atmosphere of Ar from 1323 K to 873 K at 6 K/hr, and then rapidly cooling at 50 K/hr to room temperature. A colorless, transparent $Ca_4Si_2O_7F_2$ ($Sr_4Ge_2O_7F_2$) crystal of dimensions 0.10 × 0.10 × 0.10 (0.10 × 0.12 × 0.10) mm was selected and mounted on a glass fiber with epoxy for structure determination. All measurements were made on a Rigaku AFC6R diffractometer with graphite-monochromated Mo Kα radiation. Cell constants and the orientation matrix for data collection were obtained from a least squares refinement with 20 (19) automatically-centered reflections in the range $30 \leq 2\theta \leq 36°$. The cell constants correspond to a monoclinic cell; Laue symmetry 2/m was determined on the diffractometer. Intensity data were collected over the range of indices $-10 \leq h \leq 10$, $0 \leq k \leq 14$, $-15 \leq l \leq 15$ ($0 \leq h \leq 12$, $0 \leq k \leq 18$, $-18 \leq l \leq 18$) by using the ω scan technique to a maximum 2θ value of 60°

(70°), and from 3289 (4592) measured reflections a total of 2520 (2489) were observed [$F_o^2 \geq 3\sigma F^2$]. The intensities of three representative reflections measured after every block of 200 data varied by an average of 1.6% (2%) during the collection.

The structure was solved by using the *TEXSAN* (20) software package. The crystal was found to form in the centerosymmetric space group . The positions of the Ca (Sr) and Si (Ge) atoms were derived from the direct methods program *SHELXS* (21), while the remaining atoms O and F were located from difference electron density maps. After a full-matrix least-squares refinement of the model with isotropic displacement coefficients on each atom, an absorption correction was applied (transmission factors = 0.93 - 1.10 (0.80 - 1.47)) by using the program *DIFABS* (22). The data were averaged, and the model was refined with anisotropic displacement coefficients on each atom. Final least squares refinement resulted in the residuals R = 0.027 (0.046) and R_w = 0.038 (0.051). The largest peak in the final difference electron density map corresponds to 0.16% (0.88%) of the Ca (Sr) atom. Crystal data are outlined in Table 3.1; atomic positional and thermal parameters are listed in Tables 3.2 and 3.3 .

Subsequently, all powders were prepared by mixing stoichiometric quantities of MCO_3 and $M'O_2$, heating to 1373 K, regrinding, adding stoichiometric amounts of MF_2 and heating under N_2 to 1273 K. Attempts to make $Sr_4Si_2O_7F_2$ were done in this way with 100% excess SrF_2 and 2 equivalents of LiF. All attempts were heated 1373 and 1573 K, but only starting material was observed by powder X-ray data.

Powder X-ray diffraction data were collected on a computer automated Philips diffractometer. Miller Indices for $Ca_4Ge_2O_7F_2$ were obtained by comparison to the

TABLE 3.1 Crystallographic data for $M_4M'_2O_7F_2$

chem formula	$Ca_4Si_2O_7F_2$	$Ca_4Ge_2O_7F_2$	$Sr_4Ge_2O_7F_2$
fw, u	366.48	520.51	645.65
crystal system	----------Monoclinic----------		
space group	----------$P2_1/c$ (#14)----------		
a, Å	7.534(1)	7.66	8.024(1)
b, Å	10.535(1)	10.72	11.224(1)
c, Å	10.9018(9)	11.24	11.547(2)
V, Å^3	815.6(2)	868.4	978.6(3)
β, °	109.553(8)	109.8	109.79(1)
Z	4	4	4
ρ_{calc}, g cm^{-3}	2.988		4.382
radiation	Mo Kα[a]		Mo Kα[a]
temp, K	298		298
linear abs. coeff μ, cm^{-1}	29.37		270.26
transm. factors	0.93-1.10		0.81 -1.41
R, R_w[b]	0.027, 0.38		0.046, 0.051

[a] Graphite monochromated; λ = 0.71069 Å. [b] $R = \Sigma \, | \, |F_o| - |F_c| \, | \, / \Sigma \, |F_o|$;
$R_w = [\, \Sigma w (\, |F_o| - |F_c| \,)^2 / \Sigma w \, |F_o|^2 \,]^{1/2}$.

TABLE 3.2 Positional and Equivalent Displacement Parameters (B_{eq}) for $Ca_4Si_2O_7F_2$

	x	y	z	B_{eq}
Ca1	0.02968(6)	0.08525(4)	0.81555(4)	0.67(1)
Ca2	0.16301(6)	-0.13300(4)	0.58375(4)	0.71(1)
Ca3	0.33073(6)	0.13499(4)	0.42410(4)	0.73(1)
Ca4	0.53022(6)	0.09533(4)	0.80165(4)	0.71(1)
Si1	0.65209(8)	0.19075(5)	0.12243(5)	0.51(2)
Si2	0.77281(8)	-0.19283(5)	0.86762(5)	0.52(2)
F1	0.4271(2)	-0.0038(1)	0.6012(1)	0.89(4)
F2	0.9258(2)	0.0001(1)	0.6031(1)	0.86(4)
O1	0.2297(2)	0.2197(1)	0.7548(1)	0.83(5)
O2	0.7777(2)	0.2214(1)	0.7404(1)	0.97(5)
O3	0.3007(2)	-0.0435(1)	0.8393(2)	1.12(5)
O4	0.6385(2)	0.2331(1)	0.9771(1)	0.91(5)
O5	0.5637(2)	-0.2255(2)	0.8789(2)	1.11(5)
O6	0.0900(2)	0.2352(1)	0.9910(1)	0.93(5)
O7	0.7835(2)	-0.0457(1)	0.8303(2)	1.15(5)

TABLE 3.3 Positional and Equivalent Displacement Parameters (B_{eq}) for $Sr_4Ge_2O_7F_2$

	x	y	z	B_{eq}
Sr1	0.4690(1)	0.08110(7)	0.68322(7)	0.34(2)
Sr2	0.3365(1)	-0.13231(7)	0.91678(8)	0.46(3)
Sr3	0.8310(1)	-0.13400(7)	0.92273(7)	0.36(3)
Sr4	-0.0289(1)	0.09323(7)	0.69941(7)	0.36(2)
Ge1	0.1530(1)	-0.19424(9)	0.62417(8)	0.30(3)
Ge2	0.2730(1)	0.19652(9)	0.36749(8)	0.37(3)
F1	0.0750(7)	-0.0069(5)	0.9011(4)	0.5(2)
F2	0.5738(8)	-0.0005(5)	0.8974(5)	0.8(2)
O1	0.2721(9)	0.2142(6)	0.7461(5)	0.6(2)
O2	0.7211(9)	0.2157(6)	0.7567(6)	0.6(1)
O3	0.200(1)	-0.0488(6)	0.6683(6)	1.0(1)
O4	0.135(1)	-0.2673(6)	0.9750(6)	0.8(2)
O5	0.9358(9)	-0.2662(6)	0.1232(6)	0.8(2)
O6	0.4084(9)	0.2366(6)	0.5121(6)	0.7(2)
O7	0.720(1)	-0.0498(6)	0.6750(7)	0.9(2)

diffraction pattern of the solved $Ca_4Si_2O_7F_2$ and $Sr_4Ge_2O_7F_2$ structures. Unit-cell parameters were obtained through the least squares unit-cell refinement program *Polsq* (11).

Eu^{+2} doped samples were prepared in the same way as undoped samples, except 0.03 molar equivalents MF_2 was replaced by EuF_2, and heated under a 5% H_2/Ar atmosphere. Eu^{+3} doped samples were prepared by substitution of 0.005 molar equivalents Eu_2O_3 and 0.01 molar equivalents KCl, for charge compensation, with 0.02 molar equivalents MCO_3. Luminescent spectra were collected by using the system previously described in chapter 1.

Results and Discussion

A view of the contents of the unit-cell is given in figure 3.1. The structure contains four types of M sites, one 6-coordinate, two 7-coordinate, one 8- coordinate, and two crystallographically distinct 4- coordinate M' atoms.

Selected interatomic distances and angles are listed in Table 3.4. Atom M1 is bound by one each of atoms O1, O2, O3, O6, O7, and F2 in a distorted octahedral geometry. Atom M2 is bound by one each of atoms O2, O3, O4 and O6, and F1 and two F2 atoms in an environment best described as a distorted monocapped octahedron. Atom M3 is bound to one each of atoms O1, O4, O5, O6, O7, and F2 and two F1 atoms in an environment best described as a distorted dodecahedron. The M4 atom is bonded to one each of atoms O1, O2, O3, O4, O5, O7 and F1 in a distorted monocapped octahedral geometry.

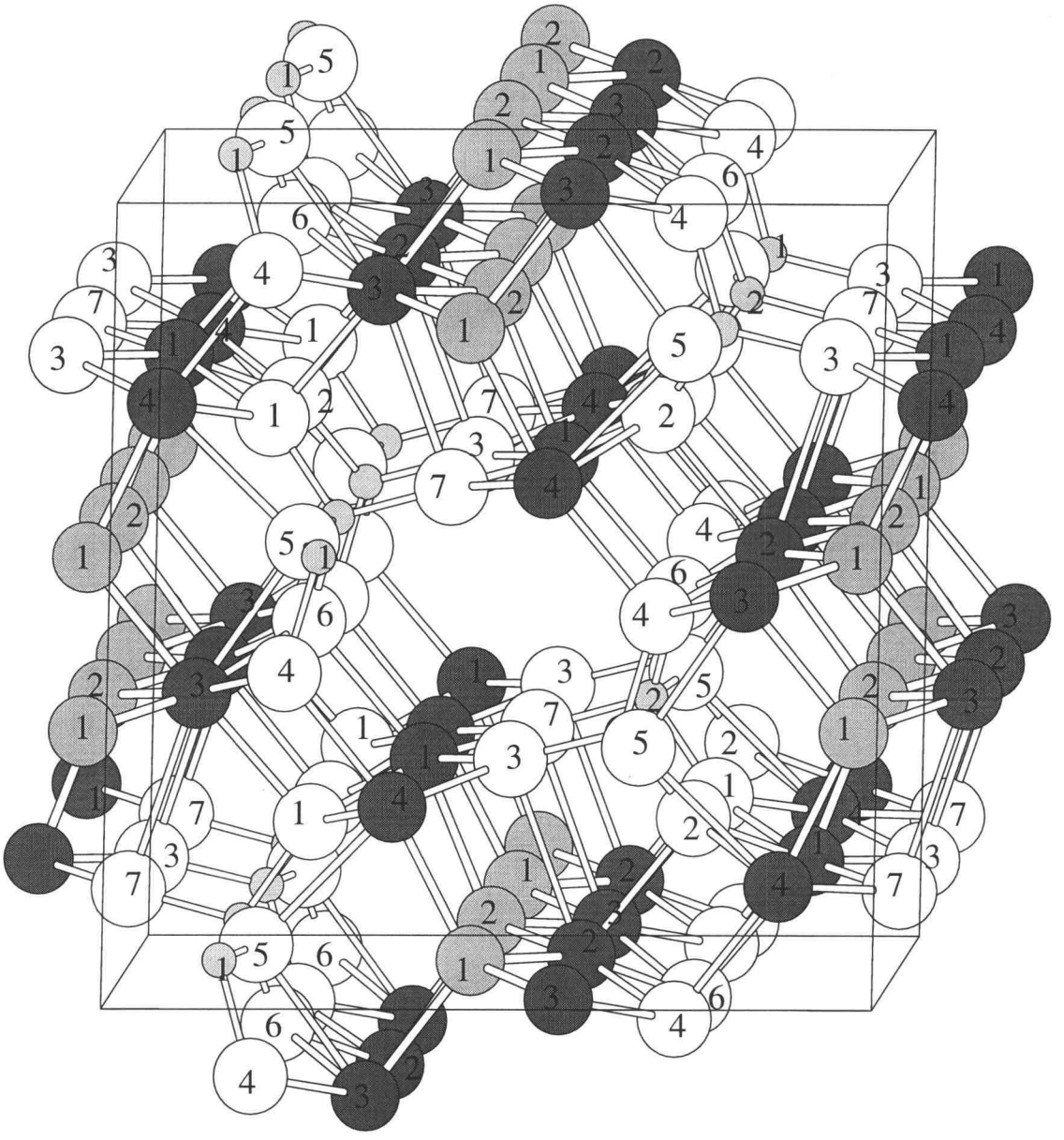

Figure 3.1. Unit-Cell diagram of $Ca_4Si_2O_7F_2$ viewed along the a axis. Open circles represent O atoms. Large dark circles represent Ca, and gray represent F atoms. Small circles represent B atoms.

TABLE 3.4 Interatomic Distances (Å) and Angles (°) for $M_4M'_2O_7F_2$.

	Ca	Sr		Ca	Sr
M-O1	2.320(2)	2.446(7)	O1-M1-O2	93.2(1)	93.4(2)
-O2	2.299(2)	2.441(8)	O1-M1-O3	76.4(1)	75.7(2)
-O3	2.392(2)	2.569(8)	O1-M1-O6	81.8(1)	80.9(2)
-O6	2.403(2)	2.562(7)	O1-M1-O7	167.8(1)	165.2(2)
-O7	2.360(2)	2.522(8)	O2-M1-O3	164.8(1)	163.4(2)
-F2	2.358(1)	2.498(6)	O2-M1-O6	77.7(1)	76.0(2)
			O3-M1-O7	79.3(1)	109.7(2)
Ave. M-O	2.355	2.508	O6-M1-O7	111.1(1)	108.3(2)
Shannon Radii[24]	2.38	2.56	F2-M1-O1	89.2(1)	87.7(2)
Ave. M-F	2.358	2.498	F2-M1-O2	85.7(1)	85.62)
Shannon Radii	2.31	2.49	F2-M1-O6	160.6(1)	157.6(2)
			F2-M1-O7	80.5(1)	79.7(2)
M2 -O2	2.375(1)	2.546(7)	O2-M2-O3	60.5(1)	61.6(2)
-O3	2.790(2)	2.864(8)	O2-M2-O4	82.67(1)	81.0(2)
-O4	2.308(2)	2.474(8)	O2-M2-O6	78.7(1)	76.7(2)
-O6	2.276(2)	2.416(8)	O3-M2-O4	115.6(1)	114.2(2)
-F1	2.365(1)	2.476(6)	O3-M2-O6	123.4(1)	122.2(2)
-F2	2.336(1)	2.479(7)	F1-M2-F2	94.0(1)	107.8(2)
-F2	2.375(1)	2.506(6)	F1-M2-O2	112.4(1)	113.3(2)
			F1-M2-O3	72.76(4)	73.1(2)
Ave M2-O	2.437	2.575	F1-M2-O4	76.5(1)	75.9(2)
Shannon Radii	2.44	2.59	F2-M2-F2	73.69(5)	73.4(2)
Ave. M2-F	2.358	2.487	F2-M2-O2	104.9(1)	105.7(2)
Shannon Radii	2.37	2.52	F2-M2-O3	75.35(5)	76.1(2)
			F2-M2-O4	168.9(1)	169.6(2)

TABLE 3.4 (Continued)

	Ca	Sr		Ca	Sr
			F2-M2-O6	79.9(1)	79.0(2)
M3 -O1	2.320(2)	2.516(7)	O1-M3-O4	81.6(1)	80.7(2)
-O4	2.597(2)	2.753(8)	O1-M3-O5	102.7(1)	102.7(2)
-O5	2.501(2)	2.635(8)	O1--M3-O6	78.4(1)	76.8(2)
-O6	2.565(2)	2.709(7)	O1-M3-O7	61.3(1)	62.7(2)
-O7	2.776(2)	2.850(8)	O4-M3-O5	59.43(5)	60.3(2)
-F1	2.334(1)	2.510(6)	O4-M3-O6	108.4(1)	108.0(2)
-F1	2.377(1)	2.487(6)	O4-M3-O7	110.98(5)	110.7(2)
-F2	2.338(1)	2.495(7)	O5-M3-O6	59.7(1)	60.0(2)
			O5-M3-O7	163.5(1)	116.5(2)
Ave M3-O	2.551	2.692	F1-M3-F1	72.16(5)	72.1(2)
Shannon Radii	2.50	2.64	F1-M3-F2	105.4(5)	107.0(2)
Ave. M3-F	2.349	2.497	F1-M3-O1	110.5(1)	112.0(5)
Shannon Radii	2.43	2.57	F1-M3-O4	70.96(5)	70.5(2)
			F1-M3-O5	113.9(1)	112.5(2)
			F1-M3-O6	98.76(5)	99.0(2)
			F2-M3-O1	105.3(1)	105.9(2)
			F2-M3-O4	173.06(5)	173.4(2)
			F2-M3-O5	118.56(5)	116.6(2)
			F2-M3-O6	74.15(5)	73.4(2)
			F2-M3-O7	72.59(5)	73.6(2)
M4 -O1	2.515(2)	2.664(7)	O1-M4-O2	111.3(1)	113.1(2)
-O2	2.553(2)	2.695(8)	O1-M4-O3	72.6(1)	72.5(2)
-O3	2.402(2)	2.539(8)	O1--M4-O4	83.4(1)	83.4(2)
-O4	2.319(2)	2.466(8)	O1-M4-O5	58.63(5)	59.2(2)

TABLE 3.4 (Continued)

	Ca	Sr		Ca	Sr
-O5	2.645(2)	2.742(8)	O4-M4-O7	103.9(1)	105.5(2)
-O7	2.355(2)	2.510(8)	O2-M4-O3	172.6(5)	170.7(2)
-F1	2.308(1)	2.459(6)	O2-M4-O4	78.791)	78.2(2)
			O2-M4-O5	58.10(5)	59.5(2)
Ave M4-O	2.465	2.603	O2-M4-O7	74.5(1)	73.7(2)
Shannon Radii	2.44	2.59	O3-M4-O4	108.3(1)	110.3(2)
Ave. M4-F	2.308	2.459	O3-M4-O5	122.2(1)	121.6(3)
Shannon Radii	2.43	2.52	O3-M4-O7	101.0(1)	99.9(2)
			O4-M4-O5	95.7(1)	99.5(2)
			O5-M4-O7	123.5(1)	122.8(2)
			F1-M4-O1	92.79(5)	92.5(2)
			F1-M4-O2	91.82(5)	92.7(2)
			F1-M4-O3	81.5(1)	79.4(2)
			F1-M4-O4	167.6(1)	167.5(2)
			F1-M4-O5	72.4(1)	72.4(2)
			F1-M4-O7	80.8(1)	79.4(2)

TABLE 3.4 (Continued)

	Si	Ge		Si	Ge
M'1 -O2	1.609(2)	1.728(8)	O2-M'1-O3	109.1(1)	108.0(4)
-O3	1.615(2)	1.712(8)	O2-M'1-O4	116.8(1)	118.5(4)
-O4	1.615(2)	1.727(7)	O2-M'1-O5	101.1(1)	99.7(3)
-O5	1.662(2)	1.799(8)	O3-M'1-O4	117.0(1)	117.9(4)
Ave. M'1-O	1.625	1.741	O3-M'1-O5	110.1(1)	110.3(4)
Shannon Radii	1.64	1.77	O4-M'1-O5	101.0(1)	100.3(4)
M'2 -O1	1.616(2)	1.727(7)	O1-M'2-O5	101.2(1)	100.1(3)
-O5	1.657(2)	1.759(8)	O1-M'2-O6	117.4(1)	117.2(3)
-O6	1.604(2)	1.722(7)	O1-M'2-O7	109.1(1)	108.5(3)
-O7	1.610(2)	1.730(8)	O5-M'2-O6	101.2(1)	100.4(4)
Ave. M'2-O	1.621	1.734	O5-M'2-O7	110.3(1)	111.2(4)
Shannon Radii	1.64	1.77	O6-M'2-O7	116.1(1)	117.6(4)

The M'1 atom is connected to one each of atoms O2, O3, O4, and O5 and the M'2 atom is bonded to one each of atoms O1, O5, O6, and O7 atoms to form slightly distorted tetrahedra. The M'1-centered tetrahedra are isolated from each other, but they connect to the M'2-centered tetrahedra through an O5 atom to form vertex-sharing dimmers M'_2O_7. See figure 3.2.

The bond-valence method (23) was used to calculate the valences of all the atoms in the structure. The fluorine atoms both have a valence within 3% (10%) of standard integral values, indicating that they have been correctly identified in the structure analysis. All the other atoms have calculated valences within 5 % of standard integral values, except for atoms O3 and O7 where valences of 1.8 (1.8), indicate lack of bonding electron density, and atom O5 where a valence of 2.2 (2.3), indicates an excess of bonding electron density.

Comparing the ratios of the M' to M atoms it is shown that sizes have an influence whether a particular combination will form. As seen in Table 3.5, the Si/Sr combination is the smallest, and we could not synthesis the $Sr_4Si_2O_7F_2$ form. This suggests that any combination of +4 metal, and +2 metal should be producible, if the ratio is at least 0.33. The upper limit has yet to be investigated.

Having a structure with distorted M sites and fluoride intermixed with oxygen surrounding metal cation, anisotropic sites for luminescence doping are available. Anisotropic site could possibly lead to unusual luminescence by relaxing the rules for electric-dipole transition in Eu^{+3}. Since the $M_4M'_2O_7F_2$ structures have 4 unique M sites, europium could have four unique emission spectra. By examining figure 3.3, the typically sharp well defined $^5D_0$-^7F_x peaks are broad and ill-defined. This suggests that multiple

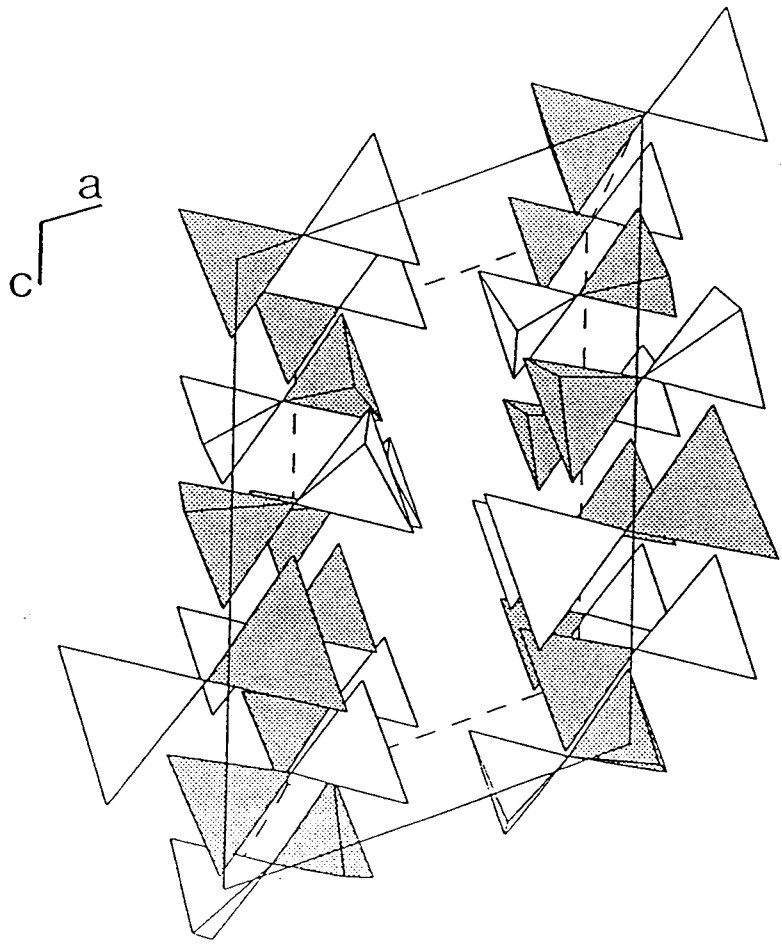

Figure 3.2 Polyhedral view along the [100] direction of the M'_2O_7 groups in $M_4M'_2O_7F_2$. Shaded tetrahedra represent $M'1O_4$ and light tetrahedra represent $M'2O_4$.

TABLE 3.5 Ratio of M'/M radii taken from Shannon (24) for 4 and 7-coordinate M' and M atoms, respectively.

	Si	Ge
Sr	0.30	0.39
Ca	0.33	0.44

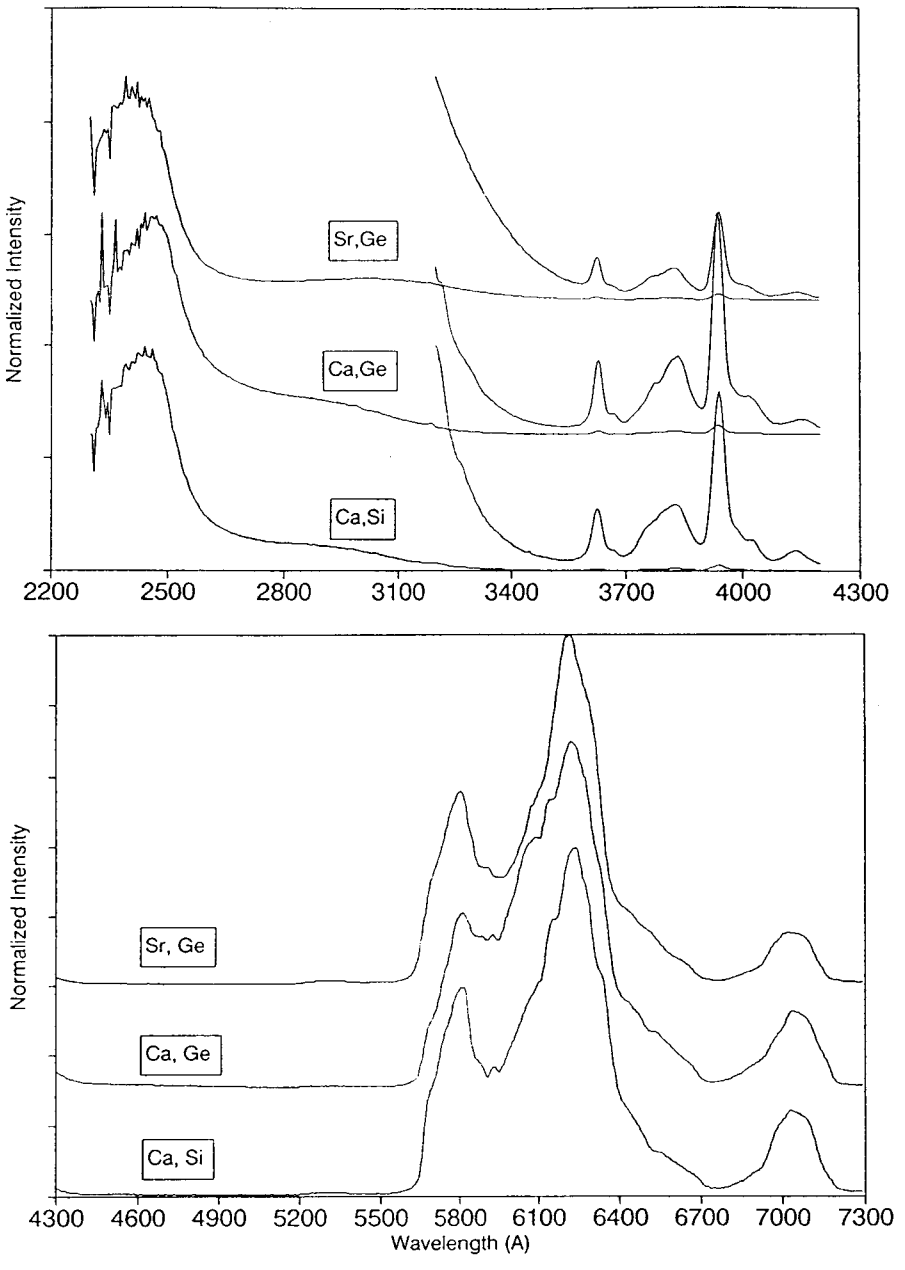

Figure 3.3 Excitation and emission spectra of the Eu^{+3} doped $M_4M'_2O_7F_2$ compounds at room temperature. Emission wavelength for excitation spectra 6230Å, excitation wavelength for emission spectra 3940Å.

europium ion transitions are overlapping. By cooling the sample and removing thermal vibration, it was thought that more detail could by seen in the spectrum. Perhaps, even the $^5D_0$-$^7F_0$ level (≈5800Å, only one peak possible for each unique Eu site) could be seen and resolved, indicating the number of unique M sites occupied by europium; However, the 4.2 K spectrum is similar to the room temperature spectrum. See figure 3.4.

As can be seen in figure 3.5, the Eu^{+2} spectra also contain typical Eu^{+3} transitions (5900-7100Å). Even though Eu^{+2} (EuF_2) was used as a starting material, and heating was done under reducing conditions, Eu^{+3} still appears in the product. Possibly $M_4M'_2O_7F_2$ is a good acid, oxidizes the Eu^{+2} and stabilizes the Eu^{+3}, or a leak in the experimental setup is allowing oxygen in. The size of the Eu^{+3} ion may be preferred compared to the Eu^{+2}, forcing oxidation; However, this would only be likely in the Ca compounds, where the Eu^{+3} is slightly smaller than Ca^{+2}, not in the Sr compounds where Eu^{+2} is the same size as Sr^{+2}. Two Eu^{+2} peaks can be seen in each of the $M_4M'_2O_7F_2$ compounds, at 4200 and 5100Å, although the intensity or the ratio of intensity varies. Since each spectrum is normalized, the relative intensity is not a good measure of the peak height for comparison to other spectra. A better reference may be the amount of noise in the spectrum, since the noise is essentially constant in all the spectra, the amount of noise seen in individual spectra indicates the intensity of the peaks (i.e. large amounts of noise in the spectrum would indicate small peaks, no noise would indicate large peaks). Since four site are possible for Eu^{+2} occupation, and only two peaks were observed, low temperature spectra were obtained. Examining figure 3.6, no splitting of the peaks is observed, but surprisingly the blue peak is thermally quenched at high temperature. Normally the larger Stokes shifted peak quenches at lower temperature because of better overlap of the excited state

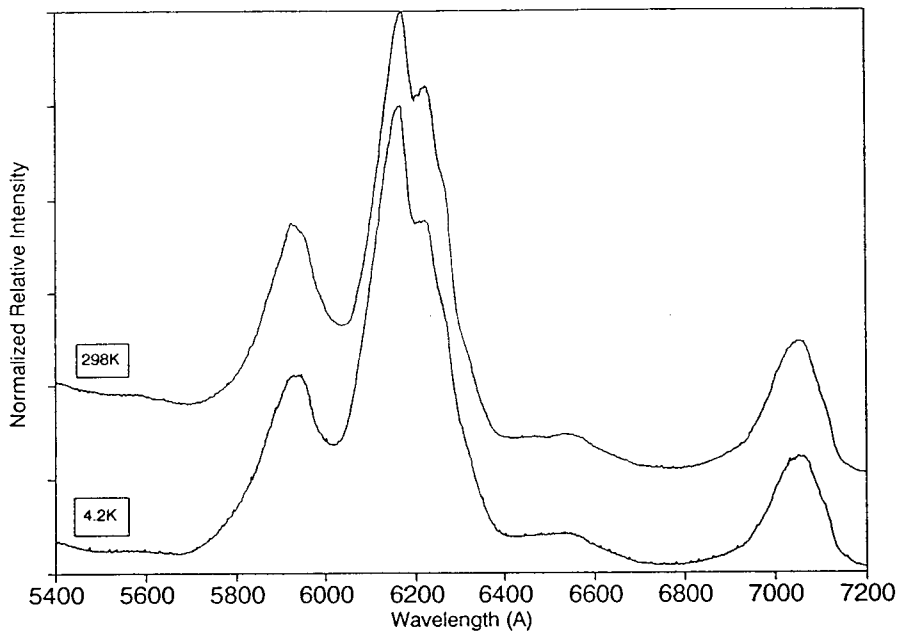

Figure 3.4. Emission spectra of the Eu^{+3} doped $Ca_4Si_2O_7F_2$ at 298 K and 4.2 K. Excitation wavelength 3940Å.

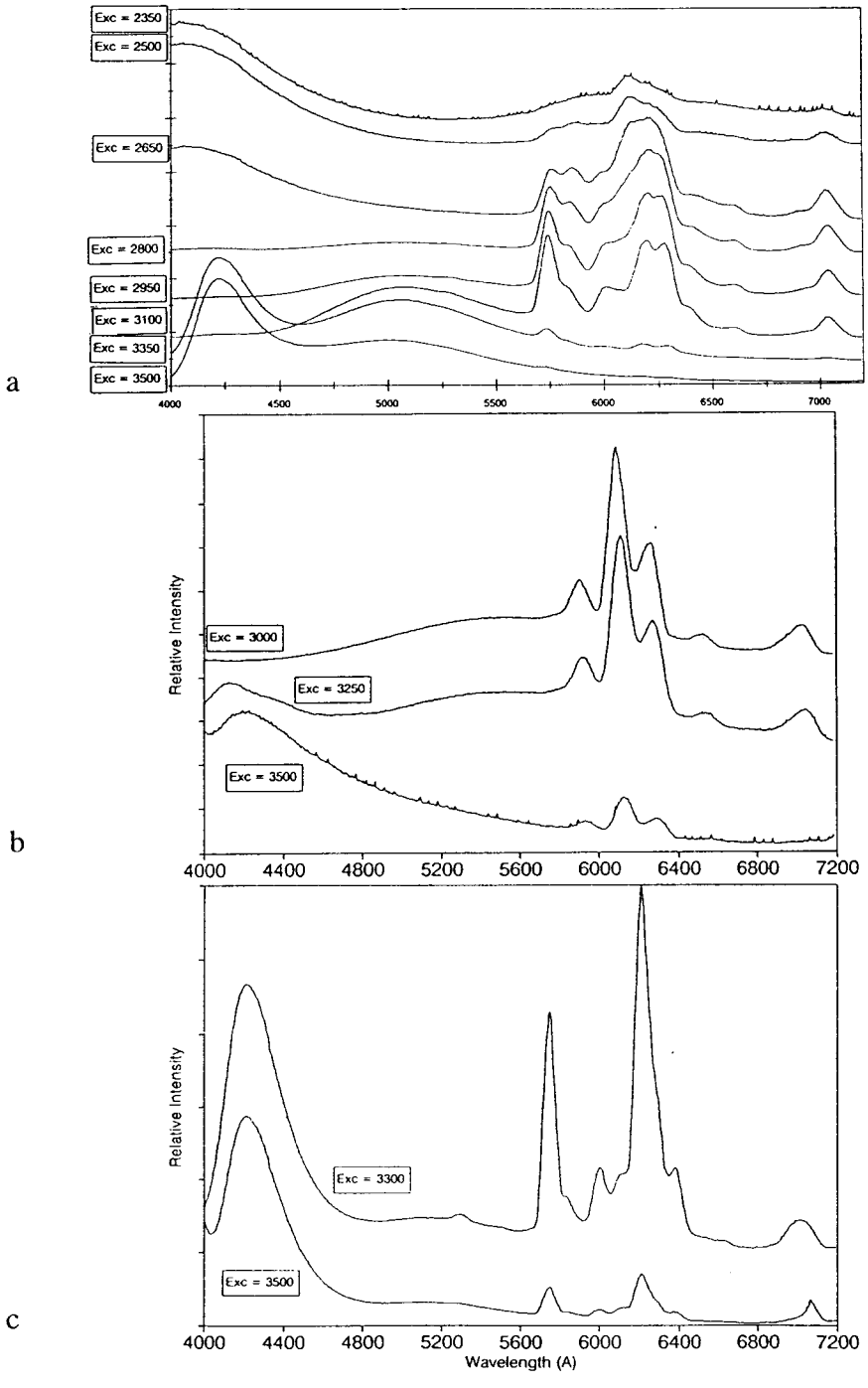

Figure 3.5 Emission spectra of the Eu^{+2} doped $M_4M'_2O_7F_2$ compounds: a) $Ca_4Si_2O_7F_2$, b) $Sr_4Ge_2O_7F_2$, c) $Ca_4Ge_2O_7F_2$. Broad peaks at 4200 and 5100Å are from Eu^{+2}, peaks at longer wavelength are typical of Eu^{+3} emission.

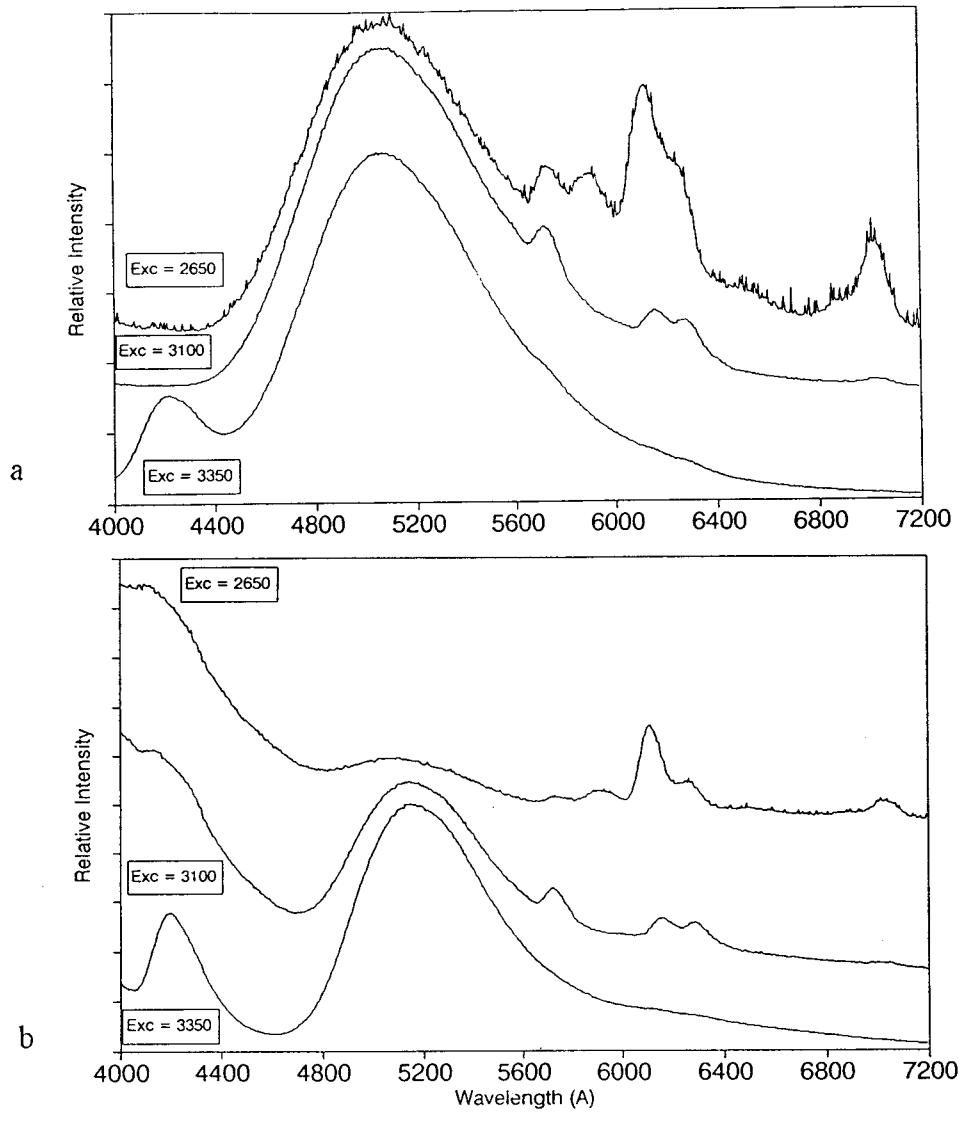

Figure 3.6 Room temperature a) and 4.2 K b) emission spectra of $Ca_4Si_2O_7F_2$ doped with Eu^{+2}. Note the ratios of the blue to the green peak.

parabola with the ground state. Two explanations seem to be possible, the excited state parabola of the blue and green emission are not the same shape, or some type of energy transfer from blue to green occurs at higher temperatures. If the green excited state parabola is very narrow, even though it is largely shifted, it may not overlap with the ground state, or the blue parabola may be very wide, and overlap well with the ground state. See figure 3.7. Both of these would lead to higher quenching temperature for green compared to blue. Transfer of energy from an excited blue site to a green site, could also be seen at room temperature, in the presents of thermal motion, and when the motion is removed by cooling the transfer also stops; however, since the Eu^{+2} concentration is less then 1%, the distance for transfer would be very large making transfer unlikely between europium ions.

Acknowledgments

This research was supported by National Science Foundation (DMR92-21372).

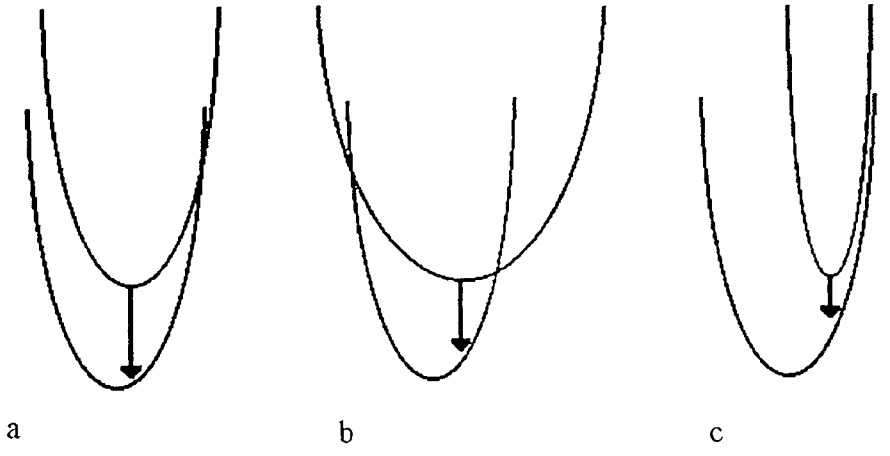

Figure 3.7 Configuration coordinate diagrams. a) Ground state and excited state parabolas are similar shape, small shift needed for overlap of edges, and some thermal energy needed for non-radiative decay. b) Excited state parabola much wider than the ground state, little or no shift needed for non-radiative decay. c) Excited state much narrower than ground state, large shift and thermal energy needed before emission is quenched.

Chapter 4
Summary

The results for the last two chapters show we have not discovered the phosphor of the century. Nevertheless, it does show how a little general knowledge of chemistry can be applied to improve current phosphors, and recognize what properties could be useful in new hosts for future applications.

The substitution of La into YBO_3 was more of a problem then it appears. The addition of the HT $LaBO_3$ and HT $NdBO_3$ phase made interpretation of data complex, and toward the end of the project it became more of a quest to figure out what was really happening throughout the entire solid solution. After correctly identify phases and peaks the data are consistent to what would be expected, and agrees well to what would be predicted from analyzing work done by Levine (25). Levine demonstrates a structure relationship to the size of the rare earth in the borate compound. YBO_3, $LaBO_3$, and $NdBO_3$ form their respective phases, but intermediate sized rare earths form one of the three phases. Comparing the average size of the Y and La, in the solid solution, to a rare earth atom of that size, agreement is reached on what the structure should be (i.e., At $Y_{0.5}La_{0.5}BO_3$ the average Y-La size is 1.02Å, similar in size to Sm, both of which form the HT $NdBO_3$ phase).

By substituting the maximum amount of La in the YBO_3 structure that is soluble, the symmetry of the Eu^{+3} site is distorted to its maximum amount. As seen in Figure 2.4, 25% La substitution can be reached at 1573 K and 1773 K. The excitation spectrum at the maximum La doping is only slightly broadened, increasing the overlap of the 1470Å

Xe emission only a few percent (5%), while the overall brightness actually dropped considerably (40%). Since La is the largest +3 ion possible to be substituted, the limit of increasing the borate absorption peak has been reached, at least by this theory. Other ways of reaching the overall goal, increasing the overlap of the 1470Å line, have yet to be investigated (substitution of the B atom?).

The emission spectra of the solid solution show improvement over the YBO_3 spectrum. Increase of the red peak is seen in all the solid solution phases. This can be attributed to the removal of symmetry around the Eu site, increasing the electric-dipole allowed transition, $^5D_0$-$^7F_2$.

The new materials, $M_4M'_2O_7F_2$ have a structure that shows interesting luminescence for Eu^{+2}, but do not have a structure allowing easily determination of what causes the unusual luminescence. The fact that the $M_4M'_2O_7F_2$ show green and blue luminescence is interesting, but having four unique M sites that Eu^{+2} can occupy does not make for an easy understanding of why. The Eu^{+3} spectra of broad overlapping peaks shows europium can be on more than one site. Other than to state that the most intense green is seen when excited at 3000Å, with a large Stokes shift to 5100Å, and the most intense blue is seen with 3500Å excitation, and a small stokes shift to 4200Å, and thermal quenching of the blue before the green is unusual, not much else can be determined. An assignment of green emission to Eu^{+2} doped on a particular M site would help in understanding why small or large Stokes shifts occur.

These results do show that the rules for Stokes shift in borates (19) could be similar for silicates. All the M sites have oxygen bonded to at least three M atoms, this would suggest that only highly Stokes shifted emission should be seen (green, but no blue);

however, since fluorine atoms are intermixed with the oxygen another influence may be involved. Also the large Stokes shift is seen for Ca compounds, where for borates it has only been seen in Sr and Ba compounds. Examining figure 3.1, M1 and M4 are only bound to one fluorine atom each, and are bound to the highly distorted O3 and O7 atoms. I would hypothesize that the green emission is coming from these sites, because of the highly asymmetric oxygen, and the lower amount of fluorine bonding.

Comparing the size ratio of the metal atoms does indicate whether isostructural compounds will form, and should make future investigations easier.

BIBLIOGRAPHY

1. Osram Sylvania Inc., 1994, *Inorganic Phosphors and Related Chemicals*, 8 ed., Towanda, Pa., 717-268-5000.

2. M.A., 1996, 'Finally, Flat TVS?', *Popular Science*, **1**, 26.

3. West, A., 1984, *Solid State Chemistry and Its Applications*, New York, NY.,Wiley and Sons.

4. Maestro, P., et al., 1992, 'Mixed Rare Earth Oxides as Starting Materials for the Preparation of Y_2O_3:Eu Lamp Phosphors: Characterization and Use', *Journal of the Electrochemical Society*, **139**, No. 5,1479.

5. West, G., et al., 1992, 'A comparison of the Eu^{3+} temperature dependent emission lifetimes in Sc_2O_3, Y_2O_3, and Gd_2O_3 Host crystals', *Journal of Luminescence*, **54**, 245.

6. Valon, P., et al., 1976, 'Synthesis of Ternary Fluorides $BaCaLn_2F_{10}$ - Eu^{2+} luminescence in $BaCaLu_2F_{10}$', *Materials Research Bulletin*, **11**, 43.

7. Weakliem, H., 1972, 'Electron Interaction in the $4f^6$ 5d Configuration of Eu^{2+} in Crystals' *Physical Review B*, **6**, No. 7, 2743.

8. Schipper. W., 1992, 'Luminescence of Eu^{2+} and Pb^{2+} Activated Alkaline-Earth Oxyhalides M_4OX_6 (M = Ca, Sr, Ba; X = Cl. Br)', *Chemistry of Materials*, **4**, 688.

9. Koike, J., et al., 1990, 'New Tricolor Phosphors For Gas Discharge Display', *Journal of the Electrochemical Society*, **126**, 1008.

10. Yoshida, Y., et al., 1995, 'Present and future of vacuum fluorescent display and field emission display', *Materials Chemistry and Physics*, **40**, 267.

11. Polsq: Least Squares Unit Cell Refinement, 1973, David Cahen.

12. CIE (Commission Internationale del' È Clairage), 1971, publication Num. 15.

13. Morgan, P.E. et al., 1977, 'Crystal Structure of $YSiO_2N$ and a Reappraisal of the "Vaterite" type, YBO_3', *Materials Research Bulletin*, **12**, 251.

14. Bradley, W.F., et al., 1966, 'The Vaterite-Type ABO_3 Rare-Earth Borates', *Acta Crystallographica*, **20**, 283.

BIBLIOGRAPHY (Continued)

15. Newnham, R.E. et al., 1963, 'Crystal Structure of Yttrium and Other Rare-Earth Borates', *Journal of the American Ceramic Society*, **46**, No. 6, 253.

16. Yamamoto, H. Matsukiyo, H., 1991, 'Problems and progress in Cathode-Ray Phosphors for High-Definition Displays', *Journal of Luminescence*, **48** and **49**, 43.

17. Abdullaev, G., 1984, 'Crystal Structure of Lanthanum Orthoborate', *Azerbaidzhanski Khimicheskii Zhurnal*, 117.

18. Bohlhoff, R., 1971, 'Die Kristallstrucktur von Hoch-$LaBO_3$', *Zeitschrift für Kristallographie*, **133**, 386.

19. Diaz, A., Keszler, D., 1996, 'Red, Green, and Blue Eu^{+2} Luminescence in Solid-State Borates: A Structure-Property Relationship'. *Materials Research Bulletin*. **31**, 147.

20. TEXSAN: Single Crystal Structure Analysis Software, Version 5.0, 1989, Molecular Structure Corp., The Woodlands, TX, 77381.

21. Sheldrick, G. 1985, SHELXS86. In *Crystallographic Computing 3*; Sheldrick, G.; Kruger, C.; Goddard, R.; Ed.; Oxford University Press: New York, 175.

22. Walker, N., Stuart, D.1983, 'An Empirical Method for Correcting Diffractometer Data for Absorption Effects', *Acta Crystallographica.*, **A39**, 158.

23. O'Keefe, M., Brese, N., 1991, 'Bond-valence Parameters for Solids'. *Journal of the American Chemical Society*. **110**, 1506.

24. Shannon, R. D., 1976, 'Revised Effective Ionic Radii and Systematic Studies of Interatomic Distances in Halides and Chalcogenides'. *Acta Crystallographica*, **A32**, 751.

25. Levine, E., et al., 1961, 'Polymorphism of ABO_3 Type Rare Earth Borates', *The American Mineralogist*, **46**, 1030.